Control of a Doubly Fed Induction Generator in a Wind Turbine During Grid Fault Ride-Through

Dawei Xiang, Li Ran, *Member, IEEE*, Peter J. Tavner, and Shunchang Yang

***Abstract*—This paper analyzes the ability of a doubly fed induction generator (DFIG) in a wind turbine to ride through a grid fault and the limitations to its performance. The fundamental difficulty for the DFIG in ride-through is the electromotive force (EMF) induced in the machine rotor during the fault, which depends on the dc and negative sequence components in the stator-flux linkage and the rotor speed. The investigation develops a control method to increase the probability of successful grid fault ride-through, given the current and voltage capabilities of the rotor-side converter. A time-domain computer simulation model is developed and laboratory experiments are conducted to verify the model and a control method is proposed. Case studies are then performed on a representatively sized system to define the feasibility regions of successful ride-through for different types of grid faults.**

***Index Terms*—Current control, doubly fed induction generator (DFIG), flux linkage, grid fault, power converter, safe operating area (SOA), wind energy.**

I. Introduction

THE doubly fed induction generator (DFIG) is a common configuration for large, variable-speed wind turbines that are connected to a grid [1]. On detecting a grid fault, the generator unit is usually disconnected to protect the vulnerable rotor-side converter. In the recent years, this has been achieved by applying a crowbar short circuit to the rotor slip ring terminals. This was accepted when wind power represented only an insignificant part of the generation in the system. As the penetration of wind power continues to increase, more wind turbines are required to remain connected during grid faults, i.e., to ride through the faults, and contribute to system stability after fault clearance [2]. For instance, the Grid Code of Scottish Power and Scottish Hydro-Electric [3] states that all wind turbines must remain connected in the event of any short circuit in the high-voltage transmission network. Grid codes in other parts of the world may be more stringent, demanding ride-through of faults at the generator terminal. For the reasons that will be discussed later, grid fault ride-through control is difficult for the DFIG and is a major challenge for wind turbine manufacturers.

Researchers are addressing the issue from several points of view. For instance, the study described in [4] suggests improving the generator terminal voltage during a grid fault using shunt reactive power compensation. Optimizing the parameters of the current control loops in the rotor-side converter is proposed in [5]. The use of the crowbar is evaluated in [6]. The inherent difficulty of ride-through control during a symmetrical grid fault is explained in [7].

It is usually thought that a fast semiconductor converter can limit the current fed to a grid fault immediately, a merit that is frequently attributed to HVDC systems [8], [9]. At first glance, it seems straightforward to apply the same principle to a DFIG, so that the rotor-side converter current could be constrained while the protection operates on impedance rather than overcurrent relays. However, in a DFIG wind turbine arrangement, the converter is on the rotor side of the generator. There are known cases where a DFIG rotor converter operated this way experienced over-voltages and failed to limit the fault current, leading to the destruction of the converter. This paper extends the initial study presented in [7] and proposes a new control approach without additional hardware but based on the insight gained from analysis and modeling backed up by experiment.

Section II of the paper reviews the generator model. The behavior of the DFIG system during a grid fault is analyzed. It is shown that the fault current depends on the internal state of the machine as well as the voltage applied on the rotor side. Section III derives the control algorithm in order to assist the system to ride through the grid fault, which takes into account the machine's internal state. Section IV verifies the proposed control method and validates the simulation model on a laboratory test rig. The validated model is used in Section V to evaluate the system performance with respect to the fault type and prefault condition. The operating region for successful ride-through for a typical 2-MW DFIG system is then defined for each fault type in terms of the severity of the fault and the prefault machine speed.

II. DFIG During Grid Fault

Fig. 1 is the block diagram of a DFIG wind turbine system. The generator has a three-phase wound rotor supplied, via slip rings, from a four-quadrant, pulse width modulation (PWM) converter with voltage of controllable amplitude and frequency. The generator can operate at variable speed, while the stator remains at a constant grid frequency. The machine usually operates in the vector-control mode orientated to the stator-flux linkage, which can be calculated as follows using the measured voltage and current [10]:

$$\psi_{sabc} = \int (u_{sabc} - R_{\mathrm{s}} i_{sabc}) dt \tag{1}$$

where ψ_{sabc} is the space vector of the flux linkages of the three-phase stator windings. u_{sabc} and i_{sabc} are the corresponding

Manuscript received July 15, 2005. The work of D. Xiang was supported by a visiting scholarship from Chongqing University, Chongqing, China. Paper no. TEC-00246-2005.

D. Xiang and S. Yang are with the Department of Electrical Engineering, Chongqing University, Chongqing 400044, China. (e-mail: xdw_cqu@hotmail.com; shunchangyang@yahoo.com).

L. Ran and P. J. Tavner are with the School of Engineering, University of Durham, Durham DH1 3LE, U.K. (e-mail: li.ran@durham.ac.uk; Peter.Tavner@durham.ac.uk).

Digital Object Identifier 10.1109/TEC.2006.875783

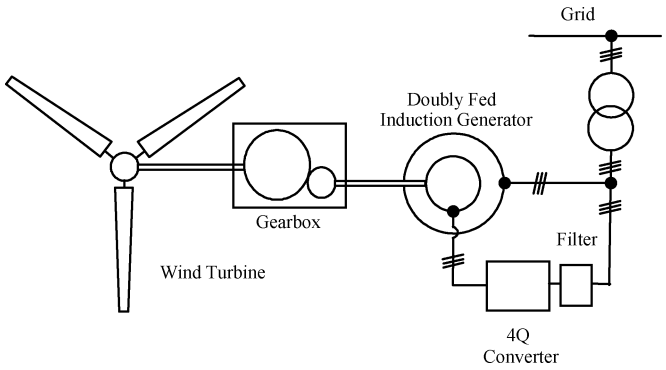

Fig. 1. Configuration of the DFIG wind turbine system.

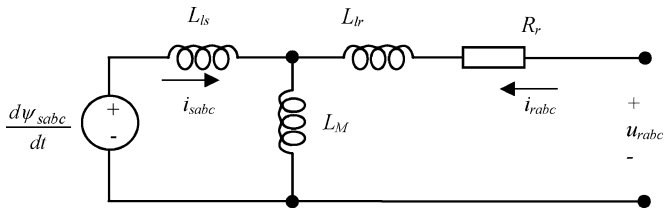

Fig. 2. Rotor-side equivalent circuit.

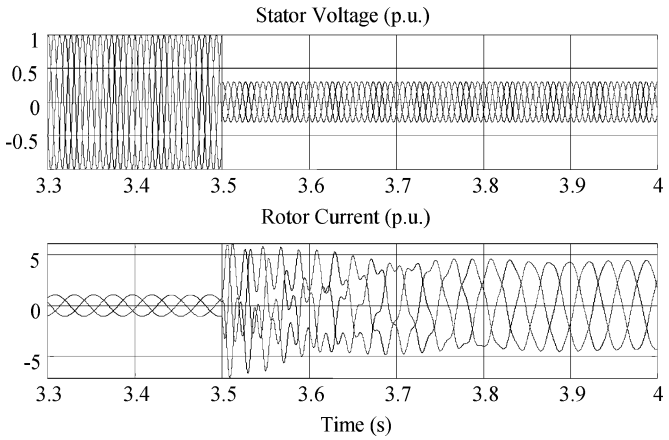

Fig. 3. Simulation results of a 2-MW DFIG during a grid fault.

voltage and current space vectors. The positive current directions are defined as feeding the generator. $R_{\rm s}$ is the stator resistance. Generally, "s" and "r" in subscript distinguish quantities or parameters on the stator or rotor side.

The stator- and rotor-flux linkages are related to the currents as

$$\psi_{sabc} = (L_{\rm ls} + L_{\rm m})i_{sabc} + L_{\rm m}i_{rabc} \tag{2}$$

$$\psi_{rabc} = L_{\rm m}i_{sabc} + (L_{\rm lr} + L_{\rm m})i_{rabc} \tag{3}$$

where $L_{\rm ls}$ and $L_{\rm lr}$ are the leakage inductances, and $L_{\rm m}$ is the magnetizing inductance. During normal operation, both the stator- and rotor-flux linkages rotate at synchronous speed with respect to the stator.

In the rotor reference frame, the voltage equation of the rotor windings is

$$u_{rabc} = R_r i_{rabc} + \frac{d\psi_{rabc}}{dt}. \tag{4}$$

The rotor-flux linkage can be expressed in terms of stator-flux linkage and rotor current according to (2) and (3) [10], [11].

$$\psi_{rabc} = \frac{L_{\rm m}}{L_{\rm s}}\psi_{sabc} + \frac{L_{\rm s}L_{\rm r} - L_{\rm m}^2}{L_{\rm s}}i_{rabc} \tag{5}$$

where $L_{\rm s} = L_{\rm ls} + L_{\rm m}$ and $L_{\rm r} = L_{\rm lr} + L_{\rm m}$. All the quantities are in per unit (p.u.).

The equivalent circuit of the DFIG machine viewed from the rotor side, corresponding to (4) and (5), is shown in Fig. 2. The rotor current is jointly decided by the injected rotor voltage and the induced electromotive force (EMF) or the derivative of the stator-flux linkage with respect to time. In normal operation, the space vector ψ_{sabc} rotates at slip speed $s\omega_0$, with respect to the rotor winding, where s is the slip and ω_0 is the synchronous speed. Therefore, ψ_{sabc}/dt is $js\omega_0\psi_{sabc}$. This is predominantly balanced by the rotor voltage of the same frequency and determines the voltage rating of the rotor-side converter, with some margin. Now consider a three-phase fault on the grid side, which brings the stator terminal voltage down to zero. In such an extreme case, the space vector of the stator-flux linkage ψ_{sabc}, will "freeze" and stop rotating with respect to the stator winding, as implied by (1). As a result, ψ_{sabc} rotates at speed $\omega_{\rm r}$ with respect to the rotor winding. The induced EMF, $d\psi_{sabc}$, will then become $j\omega_r\psi_{sabc}$, where ω_r is the rotor speed in p.u. a mismatch with the rotor supply voltage is introduced in terms of both amplitude and frequency. Current components at two frequencies, $s\omega_0$ and $\omega_r = (1-s)\omega_0$ are produced. Because the leakage inductance and rotor winding resistance are usually small, the rotor current, which is the superposition of the two components, is consequently large. With the effect of the stator resistance ψ_{sabc} will gradually decay, attenuating the transient fault current component at frequency ω_r; this is effectively the transient behavior of the rotor.

Note that the induced EMF viewed from the rotor can be relatively large during the fault because the rotor speed may be greater than the prefault slip speed. For instance, consider that the DFIG is initially running at the maximum speed, which is typically 30% above the synchronous speed [1]. The prefault slip is $s = -0.3$ p.u, while $\omega_r = (1-s)\omega_0 = 1.3\omega_0$ Correspondingly, the induced EMF increases by 333% in amplitude for the fault scenario described earlier, while the frequency also changes.

The analysis suggests that the difficulty of the rotor-side converter in constraining the current during a grid fault is associated with the induced EMF depending on the stator-flux linkage and speed. This is a major difference when compared with an inverter connected directly to a passive grid network. Fig. 3 shows the simulated fault current for a 2-MW DFIG system detailed in Appendix I. The machine initially operates with full load and is at 30% super synchronous speed. A three-phase grid fault brings the generator terminal voltage down to 0.3 p.u. The control implemented in the simulation model is the vector-control algorithm for terminal voltage regulation and the maximum active power tracking [12]. The rotor-side converter is represented

as controlled voltage sources. No additional action or control limit is included to constrain the fault current. It is observed that the rotor current increases from about 1.0 to 7.2 p.u. It is also evident that the current consists of components at different frequencies.

The analysis shows that a large rotor voltage would be required for the converter current to be constrained.

For an asymmetrical grid fault, a voltage component of negative phase sequence will appear at the generator terminal. This will cause a negative sequence component in the stator-flux linkage in addition to the dc component described earlier with respect to the stator. The rotor winding rotates with respect to the negative sequence flux component at speed $\omega_0 + \omega_r$. The corresponding EMF induced depends on the terminal voltage and the prefault machine speed. The consequence can also be explained using Fig. 2.

III. Control for Grid Fault Ride-Through

There are different interpretations to the requirements of grid fault ride-through. Ultimately, the DFIG is desired to act like a synchronous machine capable of providing fault current for protection relays and voltage support [6]. It is difficult to provide the current without increasing the converter rating. This study views the challenge of ride-through as constraining the fault current in the presence of change of the induced EMF in the machine. No additional hardware equipment, e.g., the crowbar, is to be used. In addition, the transient associated with the clearance after the fault is also to be dealt with, as the generator returns to the normal control.

The rotor-side converter usually employs the IGBT as the semiconductor switching device. Its continuous current rating is determined by the steady-state load, while the over load capability could be exploited during transient. In theory, the maximum current switched by the device can be the peak pulse rating, as long as the junction temperature reached in the IGBT is permissible and the V–I switching trajectory is within the safe operating area (SOA) [13]. The pulse current rating of an IGBT is typically 100% higher than the continuous current rating. Therefore, the control objective of this study is to constrain the instantaneous rotor current below 2.0 p.u., while the converter dc-link voltage is also maintained below the device's voltage rating. In practice, the PWM switching frequency could be temporarily reduced to prevent excessive switching losses due to increased device current and voltage during grid fault ride-through control.

A logical conclusion from the analysis in Section II is that during fault the voltage applied from the rotor converter to the rotor winding should be used to weaken the effect of the dc and negative sequence components in the stator-flux linkage. According to either (4) or Fig. 2, the effect is actually expressed through the corresponding flux components linking the rotor side. The total stator-flux linkage is dictated by the stator voltage. It is desirable to orient the rotor current such that it contains components that oppose the rotor flux linkage dc and negative sequence components. This is shown in Fig. 4, where subscripts "1," "2," and "0" indicate the positive, negative, and zero (dc) sequence components in the flux linkage or current space vectors, respectively. The converter voltage on the rotor side can be used for such an objective and the rotor current is to be kept to an acceptable limit. Whether this is achievable depends on how strongly the voltage can be applied, as compared to the internal induced EMF. The whole scenario is then dependent on the severity of the fault and the prefault condition of the DFIG system. This will be described later as the feasibility region for successful ride-through. The control approach adopted in this study aims to enlarge the feasibility region. Equation (5) can be approximated as follows:

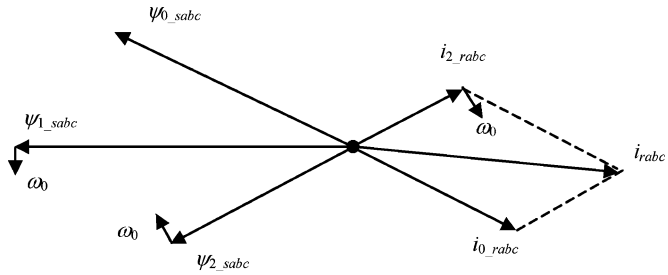

Fig. 4. Control of the rotor current.

$$\psi_{rabc} = \frac{L_{\rm m}}{L_{\rm s}}\psi_{sabc} + \frac{L_{\rm s}L_{\rm r} - L_{\rm m}^2}{L_{\rm s}} i_{rabc} \approx \psi_{sabc} + (L_{\rm sl} + L_{\rm lr}) i_{rabc}. \quad (6)$$

Equation (6) shows that the rotor current can be controlled to counter the undesired components in the stator-flux linkage. It should also be noticed that if the DFIG machine is designed with increased rotor or stator leakage inductance, it will increase the effectiveness of rotor current control and hence the ability to ride through grid faults. This is similar to the fact that a synchronous machine with increased winding leakage inductance may improve its transient behavior.

Fig. 5 shows the proposed controller including three parts: 1) stator-flux linkage estimation and decomposition; 2) calculation of rotor current reference; and 3) implementation of rotor current control. Fig. 6 shows the algorithm to decompose the stator-flux linkage vector into positive, negative, and zero sequence (dc) components. The stator voltage and current are used to calculate the total flux linkage as shown in (1). A second-order band-pass filter, whose gain and phase response are set as unity and zero degree, respectively, at the nominal stator frequency (50 Hz), is used to remove the dc component and the effect of switching harmonics. The output is ac including the positive and negative sequence components with respect to the stator winding. The dc component can therefore be calculated as follows:

$$\psi_{0\_sabc} = \psi_{sabc} - \psi_{ac\_sabc}. \quad (7)$$

It should be noted that in Fig. 6, the derivative operation has the effect of phase shifting the positive and negative sequence flux linkage components by $\pi/2$ and $-\pi/2$ (rad), respectively. The amplitude is not affected if all quantities are expressed in per

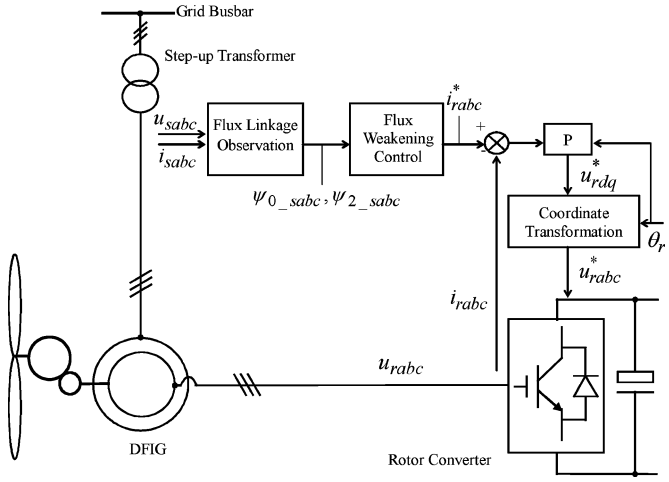

Fig. 5. Control block diagram.

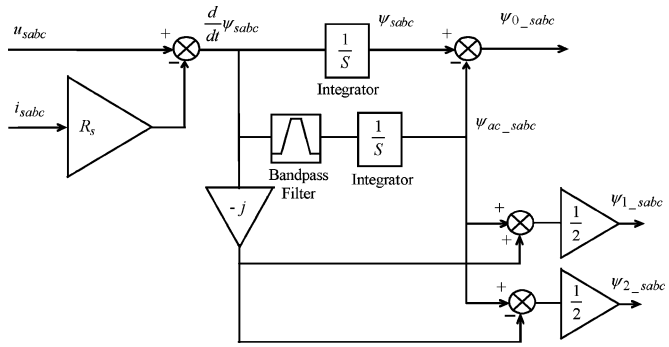

Fig. 6. Observation of components in stator-flux linkage.

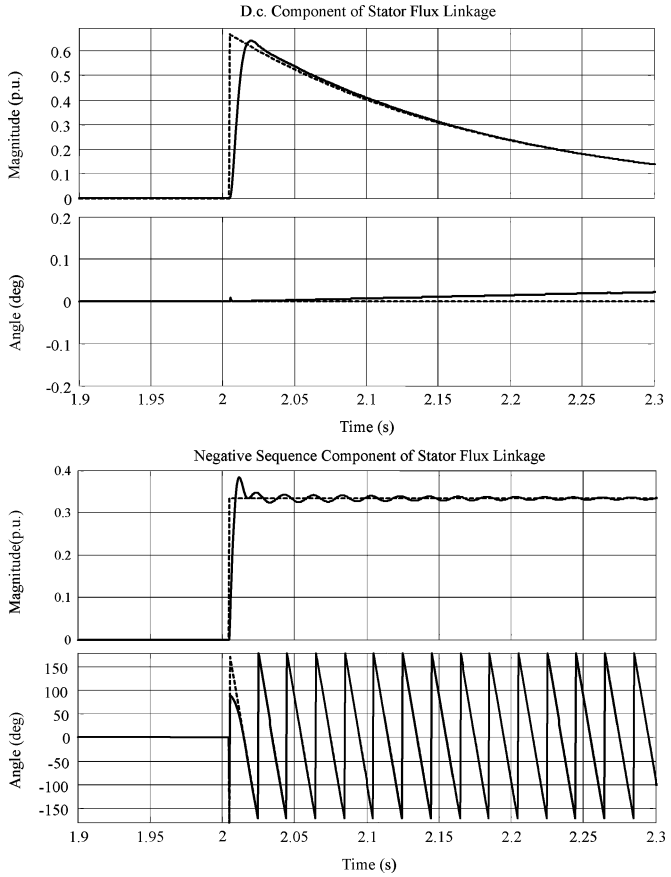

Fig. 7. Observation of components in stator-flux linkage—Test of algorithm using simulation.

unit and the system operates at the base or nominal frequency on the stator side. This is used to separate the positive and negative sequence components ψ_{1_sabc} and ψ_{2_sabc}

$$\begin{aligned}
&\frac{1}{2}\left[\psi_{ac_sabc} - (-j) \times \frac{d\psi_{sabc}}{dt}\right] \\
&\quad = \frac{1}{2}\left[(\psi_{1_sabc} + \psi_{2_sabc}) - (-j)\right. \\
&\qquad \left. \times \frac{d}{dt}(\psi_{0_sabc} + \psi_{1_sabc} + \psi_{2_sabc})\right] \\
&\quad = \frac{1}{2}[(\psi_{1_sabc} + \psi_{2_sabc}) \\
&\qquad - (-j) \times (j\psi_{1_sabc} - j\psi_{2_sabc})] \\
&\quad = \psi_{2_sabc} \qquad (8) \\
&\frac{1}{2}\left[\psi_{ac_sabc} + (-j) \times \frac{d\psi_{sabc}}{dt}\right] \\
&\quad = \frac{1}{2}\left[(\psi_{1_sabc} + \psi_{2_sabc}) + (-j)\right. \\
&\qquad \left. \times \frac{d}{dt}(\psi_{0_sabc} + \psi_{1_sabc} + \psi_{2_sabc})\right] \\
&\quad = \frac{1}{2}[(\psi_{1_sabc} + \psi_{2_sabc}) + (-j) \\
&\qquad \times (j\psi_{1_sabc} - j\psi_{2_sabc})] \\
&\quad = \psi_{1_sabc}. \qquad (9)
\end{aligned}$$

The proposed algorithm was demonstrated using simulation. A single-phase-to-ground fault on the stator side is simulated for the 2-MW DFIG system. Components in the stator-flux linkage, calculated using the above algorithm, are compared with those directly measured in the machine model. The comparison is shown in Fig. 7. The angles of the flux-linkage components are referenced to the magnetic axis of stator phase "a." Close agreement is observed with the estimation catching up the actual response in about a quarter of a 50 Hz cycle. This is because the derivative information has been taken into account in the flux-linkage observation algorithm. Control action can thus take place before the rotor current increases to an unacceptable level. Fast flux-linkage observation and rotor current response are essential to the proposed control method.

When the rotor current is used to cancel both the dc and the negative sequence components in the stator-flux linkage, it is necessary to coordinate the two aspects of the objective. The rotor current and voltage must always be within the SOA of the switching device. A series of simulations were performed to determine the appropriate sharing of the converter current

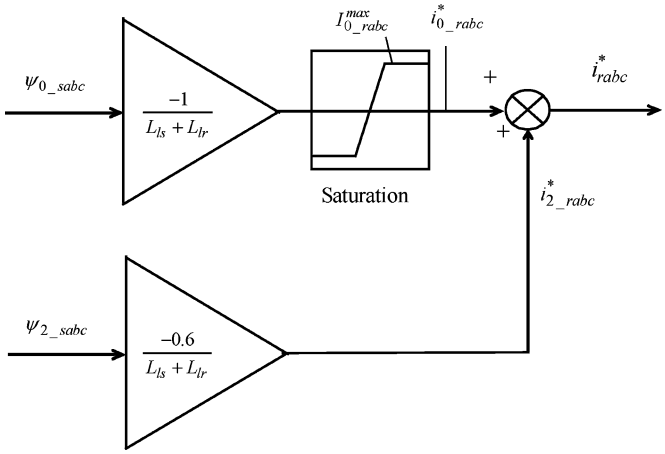

Fig. 8. Sharing of converter current capability.

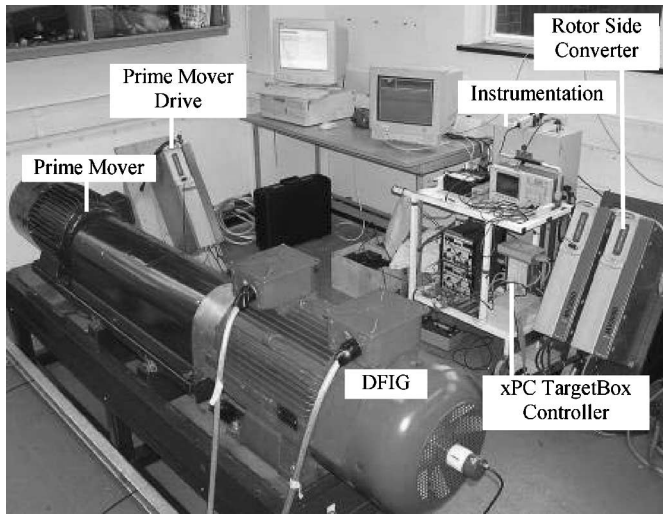

Fig. 9. Test rig setup.

capability. It was recommended to cancel 60% of the negative sequence component in the stator-flux linkage. For a typical DFIG system, this would be possible for all faults that could occur in the transmission network. The reminder of the current capability is used to deal with the dc component in the stator-flux linkage. Because the current components are at different frequencies, the maximum instantaneous current of the converter is the algebraic summation of the peak values, which must be less than 2.0 p.u. in this study. Fig. 8 shows the scheme of current capability sharing. The reference rotor current is consequently generated. The per unit limit of the dc current component is dynamically calculated depending on the negative sequence current compensation

$$I^{\max}_{0\_rabc} = 2.0 - \frac{0.6}{L_{\rm ls} + L_{\rm lr}} \left|\psi_{2\_sabc}\right|. \tag{10}$$

The implementation of the rotor current control is through a proportionalalgorithm in a stationary d–q reference frame fixed to the stator, as shown in Fig. 5. Coordinate transformation is necessary to determine the reference rotor phase voltages, taking into account the rotor angle.

IV. Experimental Verification

Fig. 9 shows the DFIG test rig set up to verify the proposed control method and the model used for full-scale system simulation. A 30-kW wound rotor machine is driven by a vector-controlled induction motor. Details of the test DFIG machine are given in Appendix III. The rotor windings of the DFIG are fed from a PWM inverter that is controlled by an xPC TargetBox real-time system. The stator and rotor currents, stator voltages and the rotor position of the DFIG machine are measured and the control algorithm described in Section III is implemented in Simulink, which generates the code to be downloaded into the xPC TargetBox. The fault occurrence is detected from a sudden change of the stator voltage, activating the fault ride-through control.

Fig. 10 shows the control response of the DFIG system during normal operation when subjected to sudden change of first real and then real and reactive power. The speed is fixed at 1950 r/min, corresponding to -0.3 p.u. slip for a four-pole machine.

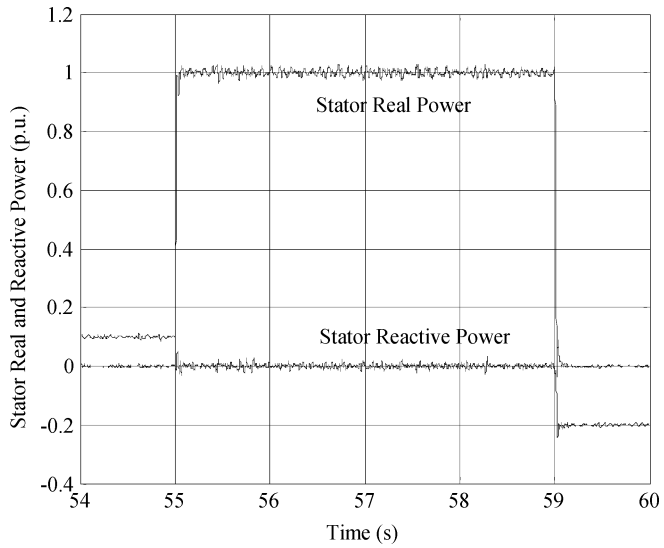

Fig. 10. Experimental results on a 30-kW DFIG control during normal operation.

The performance of fault ride-through control is verified with the DFIG initially operating with no load. The stator windings are initially open circuited and then a three-phase short-circuit fault is applied to the stator via a contactor. The unloaded machine is excited from the rotor side where the current determines the stator-flux linkage level. This is slightly different from the algorithm shown in (1) but a fault directly applied to the mains supply can be avoided. At the moment when the fault is applied to the stator, the stator-flux linkage is spontaneously trapped in the machine, giving rise to a dc component. The rotor windings then cut the trapped flux at the prefault speed, 1950 r/min in this experiment. The control objective is to constrain the rotor current in the presence of the induced EMF. The experiment setup is thus adequate to verify the proposed control method.

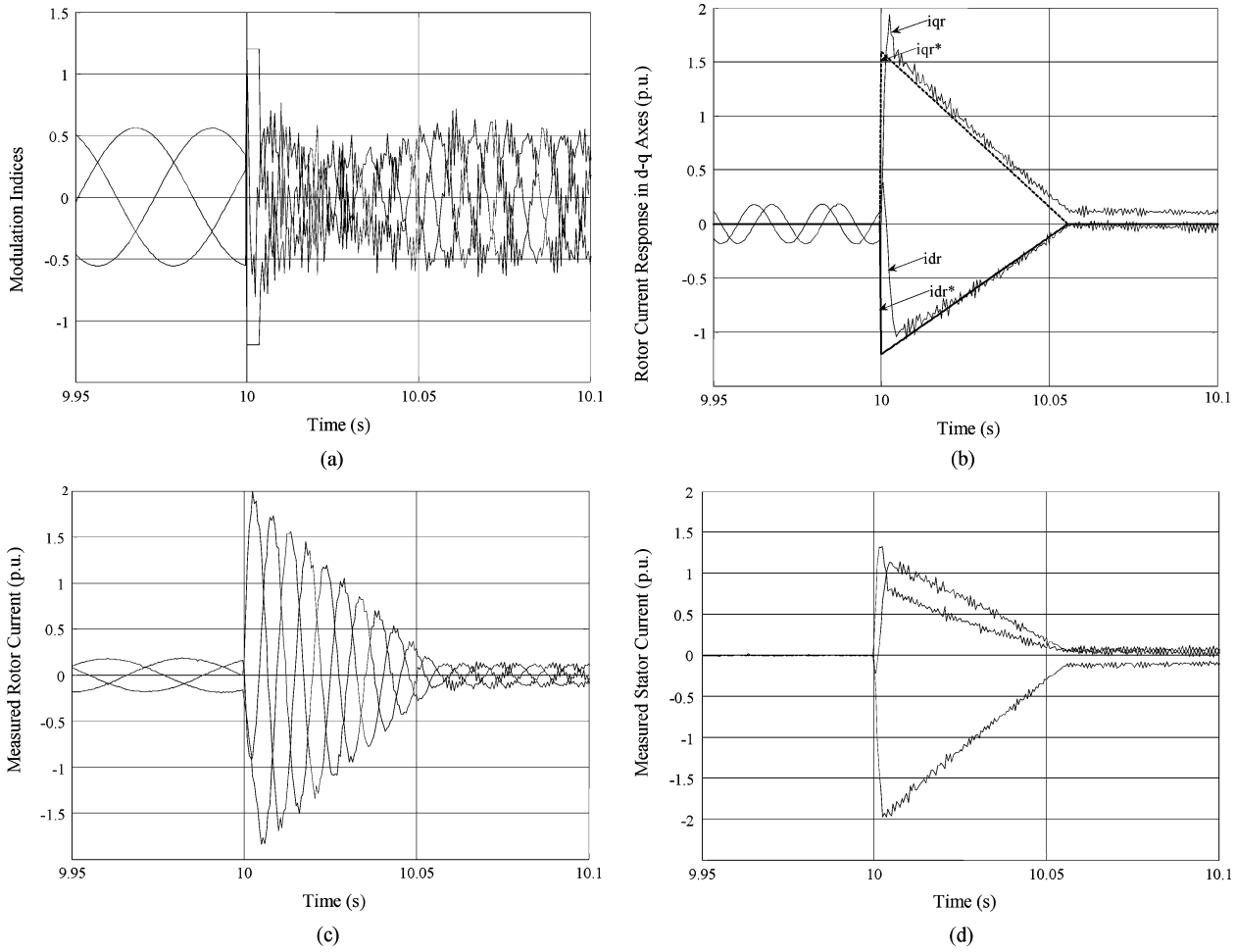

Fig. 11. Experimental results on a 30-kW DFIG with ride-through control.

Upon detecting the fault, the rotor current is controlled to oppose the dc component of the stator-flux linkage. The latter will decay due to the winding resistance. It can be shown that, without control action, it decays exponentially with the stator short-circuit time constant [14]

$$\tau_s' = \left[1 - \frac{L_{\rm m}^2}{(L_{\rm ls}' + L_{\rm m})(L_{\rm lr}' + L_{\rm m})}\right] \frac{L_{\rm ls}' + L_{\rm m}}{R_{\rm s}'} \qquad (11)$$

where $L_{\rm ls}'$ and $R_{\rm s}'$ include the contribution from the grid. The dc component of the stator-flux linkage decays more rapidly under control. In practice, the control gains should be enough for the flux to decay to nearly zero by the time when the fault is cleared. The compensating current component should decay correspondingly. In the experiment, the current decrease is represented in the control algorithm using a simple linear approximation.

Fig. 11 shows a set of experimental results where the decrease of the reference rotor current takes place in 55 ms. The initial compensation level is 2.0. p.u. in terms of the rotor current. The prefault rotor excitation level is set so that the stator voltage is initially 0.7 p.u. Fig. 11(a) shows the three-phase PWM modulation indices, which are to be compared with the triangular carrier between [-1, 1]. It is clear that overmodulation is required to increase the inverter output voltage while the dc link in this experiment is kept constant. Fig. 11(b) shows the response of the rotor current in the d–q reference frame where the d-axis coincides with stator phase "a" and the q-axis leads the d-axis by 90°. The small steady-state error is due to the proportional control and cross coupling between the two axes [15], which is not compensated in the study as the control is only for a short period of time. A small steady-state error is considered acceptable in this study. The three-phase rotor currents are also directly measured as shown in Fig. 11(c). While the envelope of the rotor current follows the desired profile, it is observed that the frequency changes from the prefault slip frequency (-0.3 p.u.) to a higher value (1.3 p.u.). Finally, Fig. 11(d) shows the measured response of the stator current. In this particular case, the stator current contains only the dc component during the fault.

Fig. 12 shows the simulation results corresponding to the experimental system, which indicates close agreement with the test although the fault occurs at a different phase angle on the waveforms. The experiment therefore verifies the simulation model, which can then be confidently used in full-scale system studies.

In both the experimental and the simulation results, the converter or rotor current is successfully constrained in 2.0 p.u. Note that the base voltage and current in Appendix III are purposely reduced as compared to the machine or converter rating to provide a safety margin. The rotor voltage also reaches the maximum that could be provided by the converter with

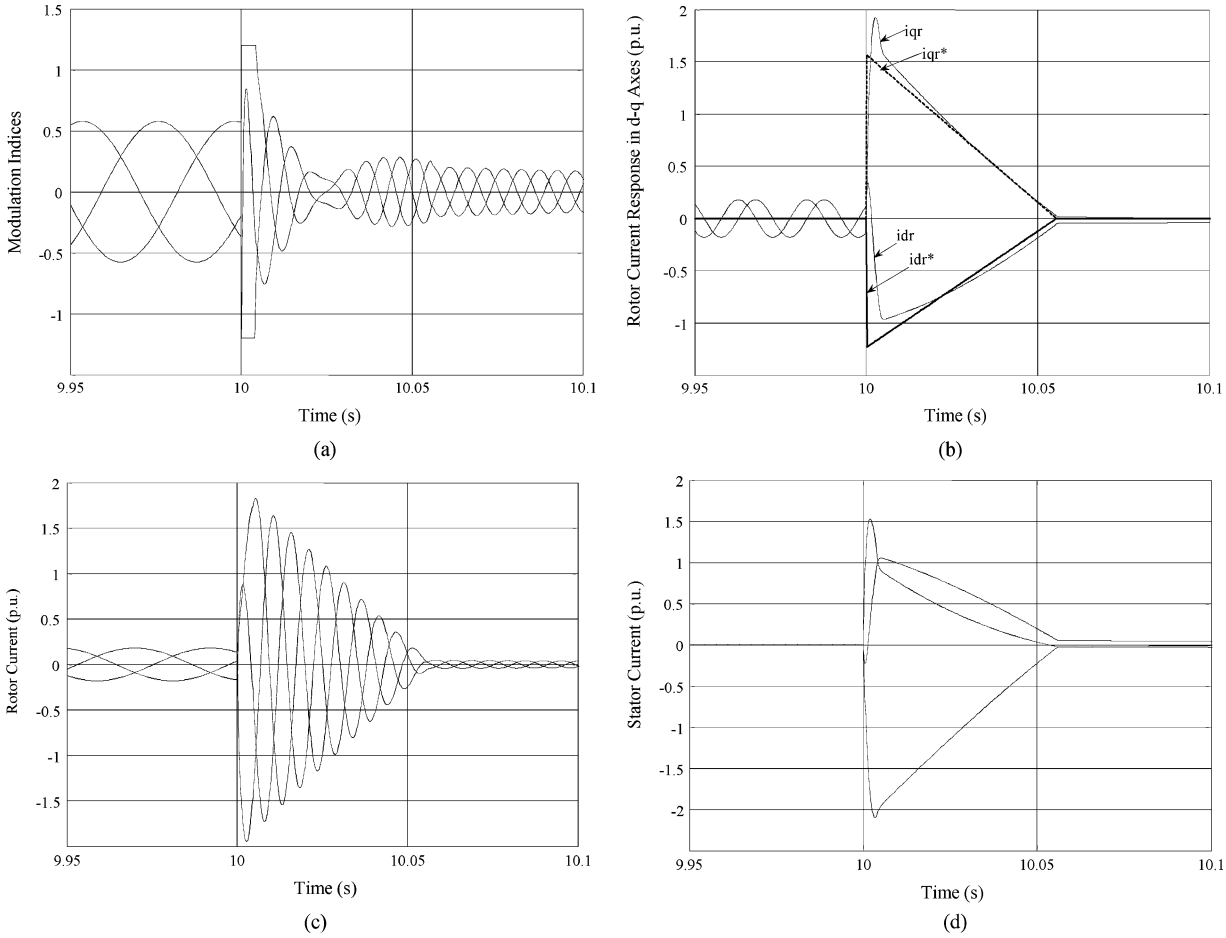

Fig. 12. Simulation results on a 30-kW DFIG with ride-through control.

overmodulation. Further experiments showed that for the same control setup, the current cannot be constrained if the prefault stator voltage is increased. This indicates that the success for the DFIG to ride through the fault depends on the dc component of the flux linkage trapped in the machine. As the prefault voltage increases, more flux is trapped increasing the induced EMF. The experimental results showing the effect of the prefault condition are summarized in Fig. 13.

V. Simulation Studies and Feasibility Regions

The verified model is used to simulate the ride-through control of the DFIG in different fault scenarios with a full-size machine. Fig. 14 shows a hypothetic network configuration of the 2-MW DFIG used in this study. The parameters of the step-up transformer and the double-circuit transmission network are given in Appendix II. From the generator point of view, the severity of the fault depends on the fault type and its distance from the generator terminal. Given the fault type, an index is defined to indicate the severity. The smaller is the $K_{\rm f}$, the more severe is the fault.

$$K_{\rm f} = \frac{Z_2}{Z_2 + Z_3}. \tag{12}$$

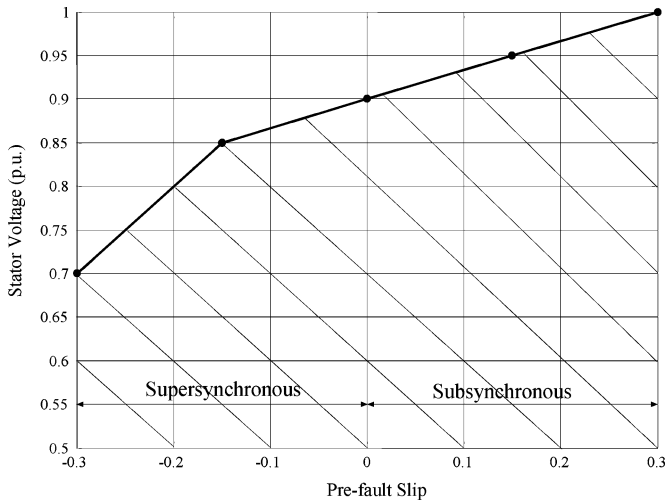

Fig. 13. Feasibility region (shaded) for ride-through control obtained from experiments.

A. Three-Phase Fault

Simulation is performed with $K_{\rm f} = 0.25$ and the results are shown in Fig. 15. The maximum slip is $s = \pm 0.3$ p.u. The

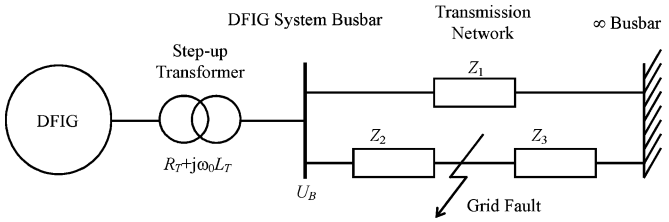

Fig. 14. Configuration of a simulated 2-MW DFIG system.

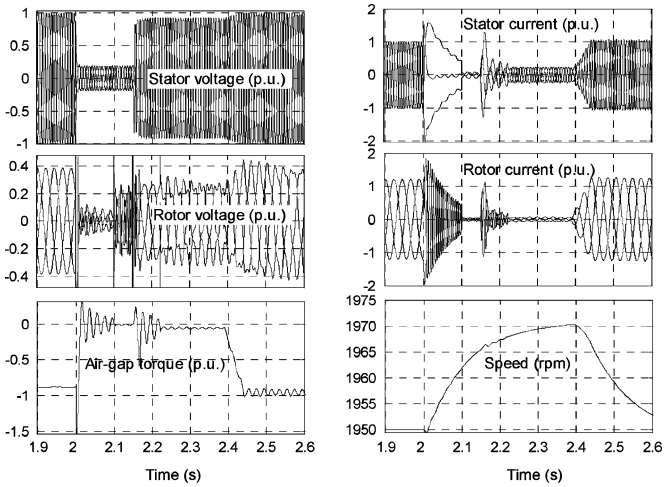

Fig. 15. Simulation results on a 2-MW DFIG for a three-phase fault.

rotor voltage, approximately $s\omega_0\psi_{rabc}$, is about 0.3 in the per unit system chosen in this study assuming 1.0 p.u. rotor flux linkage [16]. This means that the maximum rotor voltage will be around 0.43 p.u. with overmodulation [13].

The three-phase fault occurs at $t = 2$ s and it is assumed that the faulty transmission circuit is tripped after $t = 2.1$ s. The DFIG wind turbine initially runs at the nominal speed (1950 r/min) and the generator is almost fully loaded with a lagging power factor of 0.867. Fig. 15 shows that at the fault occurrence, the rotor current is constrained in 2.0 p.u. From $t = 2.1$ s, the reduced rotor current is forced to nearly zero, waiting for the fault to be cleared. As the dc component in the flux linkage would have reduced at this stage, it should be possible for the rotor converter to provide the voltage needed to null the current. At $t = 2.15$ s, the fault is cleared and the stator voltage recovers. The same concept of ride-through control is applied to the transient of fault clearance, which also introduces undesired components in the stator-flux linkage. From $t = 2.15$ s to $t = 2.25$ s, the rotor current is again controlled to weaken the dc component in the stator-flux linkage. It is controlled to zero after $t = 2.25$ s. At $t = 2.4$ s, the ride-through control is then disabled while the normal vector control is enabled. The air-gap torque is again developed.

Sensitivity studies were performed to investigate the factors that affect the ride-through control. The following changes in the prefault condition will make it more difficult to ride through the grid fault: 1) increase of machine speed and 2) increase of the reactive power generated by the DFIG on the stator side.

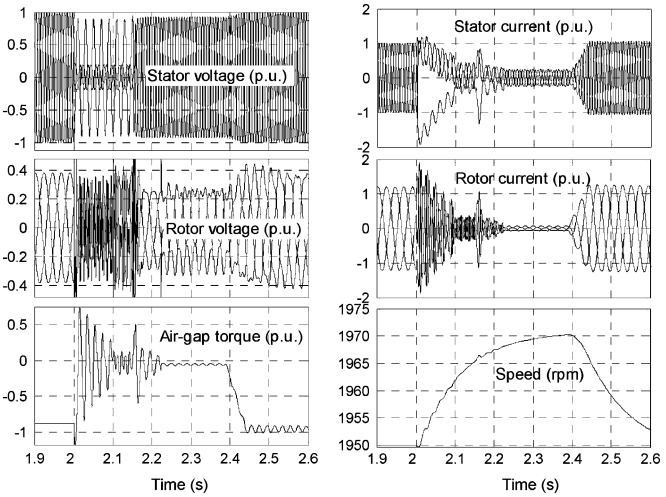

Fig. 16. Simulation results on a 2-MW DFIG for a phase–phase–ground fault.

This is consistent with the analysis on the mechanism of ride-through control since both of them increase the fault-induced EMF in the machine.

B. Phase–Phase–Ground Fault

Fig. 16 shows the simulation results with a phase–phase–ground fault in the network. Again, $K_{\rm f} = 0.25$. The prefault condition is the same as that given earlier.

Although the fault type is rare in practice, this case shows the features in an asymmetrical fault.

Compared with the previous case of symmetrical fault, the main difference is that a negative sequence component now exists in the stator-flux linkage during the transient. Part of the rotor current is utilized to cancel the effect of this component. However, as the cancellation is not complete, this leads to a new component induced in the rotor voltage, whose frequency is $2 - s$ p.u. As a result of the induced voltage, the maximum instantaneous value of the required rotor voltage may be higher than that used for the control. With interactions between the dc, positive-, and negative-sequence components in the flux linkages, the air-gap torque also has additional harmonic content not present previously.

In practice, an area of concern with an asymmetrical fault is the stabilization of the converter dc-link voltage. This was checked in simulation and it was found that the grid side converter could be controlled to avoid over current in the presence of unbalanced grid side voltage [17]. In general, with the proposed control of the rotor-side converter, the exchange of real power across the converter is also attenuated during the fault. The dc-link voltage can be readily stabilized for the fault scenario simulated.

C. Feasibility Region

Ride-through control is affected by many factors; the study identified that the most important ones are the prefault speed and the severity of the fault. The feasibility region for the DFIG to successfully ride through a grid fault is therefore investigated

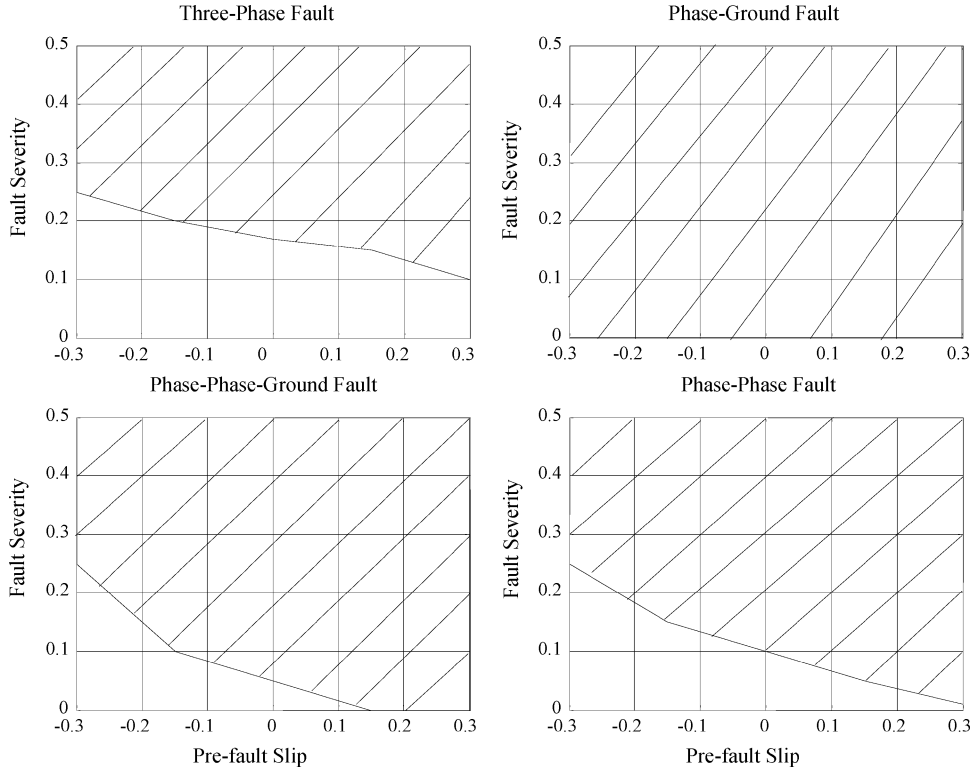

Fig. 17. Feasibility regions of grid fault ride-through (shaded) obtained from simulation.

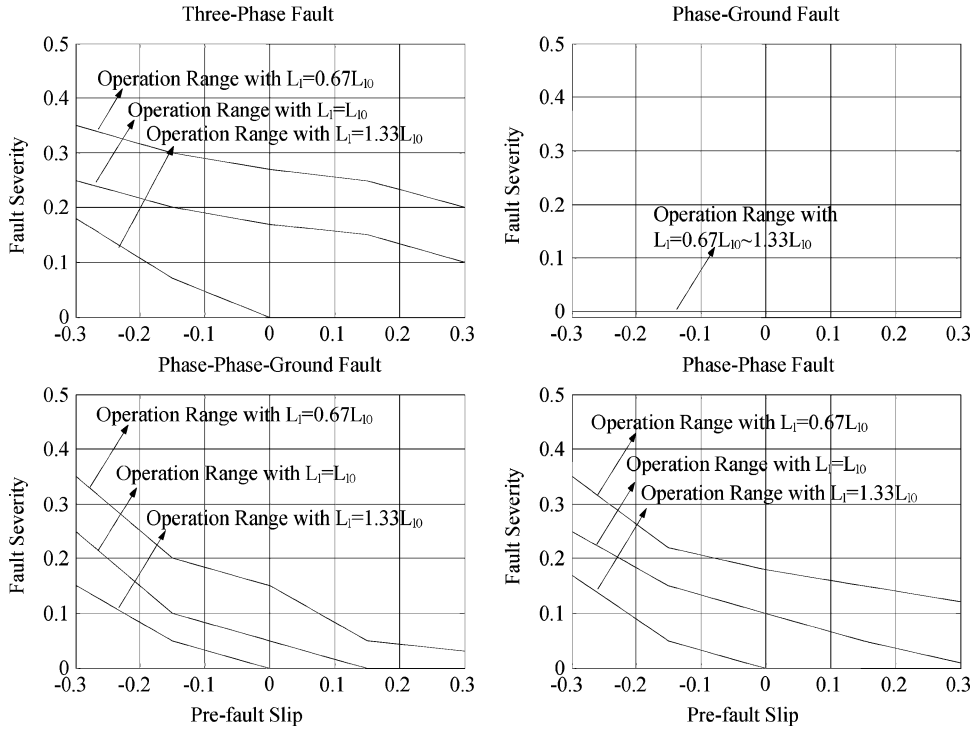

Fig. 18. Effect of machine leakage inductance on the feasibility region.

for each type of fault with respect to the prefault speed and K_{f}, to define the boundary that separates the situations that the DFIG can handle from those that it cannot and hence must be disconnected. The criterion is based on whether the rotor current can be constrained to 2.0 p.u. with a rotor voltage that is instantaneously lower than 0.43 p.u. as argued in Section V-A.

The feasibility regions identified are shown in Fig. 17. The slip covers the whole normal speed range, which is $\pm$ 30%

around the synchronous speed. The power factor on the stator side of the machine is fixed at 0.867 lagging. The total DFIG power changes with the speed and is shared between the stator and rotor circuits according to the slip [1]. In Fig. 17, any point in the shaded area means that the DFIG can ride through the grid fault in the corresponding condition. For any fault type, it is generally more difficult to ride through the fault of the same severity when the generator operates at a higher speed. When the generator operates at a speed 30% above the synchronous speed, i.e., -0.3 slip, it can ride through a symmetrical three-phase as long as the severity index is not less than 0.25 corresponding to the terminal voltage of about 0.3 p.u.

It is clear from Fig. 17 that the DFIG can ride through all single-phase-to-ground faults in the transmission network. This conclusion is however only valid for the specific system under study and the ride-through criterion described earlier. If the system configuration changes or the current and voltage capabilities of the converter are set differently, the feasibility regions for all fault types need to be revised.

As pointed out in the theoretical analysis in Section III, the DFIG ride-through control favors increased leakage inductance of the machine. Fig. 18 shows the feasibility regions as affected by total stator and rotor leakage inductance $L_{\rm l} = L_{\rm ls} + L_{\rm lr}$. Originally, $L_{\rm ls} = 0.1386$ p.u., $L_{\rm lr} = 0.1493$ p.u., and the total $L_{10} = 0.2879$ p.u. $L_{\rm ls}$ and $L_{\rm lr}$ are proportionally scaled to change the total leakage inductance. It is confirmed that increased leakage inductance indeed increases the feasibility regions. In practice, the stator and rotor leakage inductance can be increased by the choice of the slot depth, slot wedge, and the end winding arrangement [18]. An overall optimized solution should however be reached after also considering other effects, for example, the reactive power losses in the machine during normal operation.

VI. Conclusion

This paper analyzes the challenge for a DFIG wind turbine to ride through a grid fault. It has been shown that dc and negative sequence components are caused in the machine flux linkages, resulting in a large EMF induction in the rotor circuit. A new method is proposed to control the rotor-side converter so that the rotor current contains components to oppose the undesired components in the stator-flux linkage. Fast observation of the stator-flux linkage components is essential to the control, which effectively constrains the rotor current given the voltage capability of the converter. A test rig has been set up to verify the analysis and a control method has been proposed. Simulations based on a validated model provide the feasibility regions, in terms of fault severity and prefault speed, of successful ride-through control for a 2-MW DFIG connected to the grid through a double-circuit network. It is shown that the maximum turbine speed sets the most demanding scenario for ride-through control for all fault types. Increased machine leakage inductance is useful to the ride-through control method proposed.

The study clearly shows the ability for a DFIG wind turbine generator to ride through the grid fault and the limitations to that control objective. The study can be extended to evaluate the wind farm design, or to identify the situations where additional means of control and protection must be provided.

Appendix I

2-MW Machine Equivalent Circuit Parameters

Ratings: $S_{\rm n} = 2.0$ MW, $f_{\rm n} = 50$ Hz, $U_{\rm n} = 690$ V (line–line, rms), four pole
Winding connection (stator/rotor): Y–Y
Turns ratio: $N_{\rm s}/N_{\rm r} = 0.45$
Stator resistance: $R_{\rm s} = 0.00488$ p.u.
Stator leakage inductance: $L_{\rm ls} = 0.1386$ p.u.
Rotor resistance: $R_{\rm r} = 0.00549$ p.u.
Rotor leakage inductance: $L_{\rm lr} = 0.1493$ p.u.
Magnetizing inductance: $L_{\rm m} = 3.9527$ p.u.
$H = 3.5$ s
Base capacity: $S_{\rm b} = 2$ MVA
Base frequency: $f_{\rm b} = 50$ Hz
Base stator voltage (phase, peak value): $V_{\rm sb} = 563.4$ V
Base rotor voltage (phase, peak value): $V_{\rm rb} = 1252$ V
Proportional gain of current control: $K_{\rm p} = 1.6$

Appendix II

2-MW DFIG Transformer and Transmission Network Parameters

$S_{\rm n} = 2.5$ MW, $f_{\rm n} = 50$ Hz
Primary winding: 20 kV-Δ
Secondary winding: 690 V-Y0
Short-circuit impedance: $Z_{\rm T} = 0.0098 + j0.09241$ p.u.
Transmission line impedance: $Z_1 = Z_2 + Z_3 = 0.01 + j0.1$ p.u.
Base capacity: $S_{\rm b} = 2.5$ MVA

Appendix III

Test Rig DFIG Machine Parameters

Ratings: $S_{\rm n} = 30$ kW, $f_{\rm n} = 50$ Hz, $U_{\rm n} = 400$ V (line-line, rms), four pole
Winding connection (stator/rotor): Y–Y
Turns ratio: $N_{\rm s}/N_{\rm r} = 400/380$
Stator resistance: $R_{\rm s} = 0.0404$ p.u.
Stator leakage inductance: $L_{\rm ls} = 0.0673$ p.u.
Rotor resistance: $R_{\rm r} = 0.0315$ p.u.
Rotor leakage inductance: $L_{\rm lr} = 0.1152$ p.u.
Magnetizing inductance: $L_{\rm m} = 3.8997$ p.u.
Base capacity: $S_{\rm b} = 2.887$ kVA
Base frequency: $f_{\rm b} = 50$ Hz
Base stator voltage (phase, peak value): $V_{\rm sb} = 81.65$ V
Base rotor voltage (phase, peak value): $V_{\rm rb} = 77.57$ V
Proportional gain of current control: $K_{\rm p} = 1.6$
dc-link voltage: 48 V

Acknowledgment

The authors would like to acknowledge ALSTOM Power Conversion and FKI-DeWind for providing the test rig equipment. They would also like to thank several colleagues

for the help they provided during the study, particularly Dr. J. Bumby and Dr. P. Taylor of Durham University, Durham, U.K.; Dr. S. Finney of Heriot-Watt University, Edinburgh, U.K.; and Dr. X. Yuan of GE-Shanghai, Shanghai, China.

REFERENCES

[1] S. Muller, M. Deicke, and R. W. De Doncker, "Doubly fed induction generator systems for wind turbine," *IEEE Ind. Appl. Mag.*, vol. 8, no. 3, pp. 26–33, May–Jun. 2002.
[2] P. Fairley, "Steady as she blows," *IEEE Spectr.*, vol. 40, no. 8, pp. 35–39, Aug. 2003.
[3] J. L. Dallachy and I. Tait, "Guidance note for the connection of wind farms," 2.2.2, *SP Transmission and Distribution, Scottish Hydro-Electric*, 2002.
[4] O. Anaya-Lara and N. Jenkins, "Fault current contribution of DFIG wind turbines," presented at the IEE Conf. Reliability of Transmission and Distribution Networks, London, Feb. 2005.
[5] A. Petersson, L. Harnefors, and T. Thiringer, "Evaluation of current control methods for wind turbines using doubly-fed induction machines," *IEEE Trans. Power Electron.*, vol. 20, no. 1, pp. 227–235, Jan. 2005.
[6] G. Pannell, D. Atkinson, R. Kemsley, L. Holdsworth, P. Taylor, and O. Moja, "DFIG control performance under fault conditions for offshore wind applications," presented at the CIRED Conf., Turin, Italy, Jun. 2005.
[7] D. Xiang, L. Ran, P. J. Tavner, and J. R. Bumby, "Control of a doubly fed induction generator to ride through a grid fault," presented at the Int. Conf. Electric Machines (ICEM), Cracow, Poland, Sep. 2004.
[8] N. M. Kirby, L. Xu, M. Luckett, and W. Siepmann, "HVDC transmission for large offshore wind farms," *Power Eng. J.*, vol. 16, no. 3, pp. 135–141, Jun. 2002.
[9] U. Axelsson, A. Holm, C. Liljegren, K. Eriksson, and L. Weimers, "Gotland HVDC light transmission—world's first commercial small scale dc transmission," presented at the CIRED Conf., Nice, France, May 1999.
[10] P. C. Krause, *Analysis of Electrical Machinery*. Piscataway, NJ: IEEE Press, 1995, pp. 164–178.
[11] P. Vas, *Vector Control of AC Machines*. Oxford, U.K.: Oxford Univ. Press, 1990, pp. 39–40.
[12] R. Pena, J. Clare, and G. Asher, "Doubly fed induction generator using back-to-back converters and its application to variable-speed wind-energy generation," *IEE Proc.-Elect. Power Appl.*, vol. 143, no. 3, pp. 231–241, May 1996.
[13] N. Mohan, T. M. Undeland, and W. Robbins, *Power Electronics: Converters, Applications and Design*. New York: Wiley, 2003, pp. 626–637, 208–210.
[14] D. W. Novotny and T. A. Lipo, *Vector Control and Dynamics of AC Drives*. Oxford, U.K.: Oxford Univ. Press, 1996, p. 178.
[15] L. Ran and Y. Liao, "Sampling-induced resonance in an encoderless vector controlled induction motor drive," *IEEE Trans. Ind. Electron.*, vol. 51, no. 3, pp. 551–557, Jun. 2004.
[16] M. S. Vicatos and J. A. Tegopoulos, "Transient state analysis of a doubly-fed induction generator under three phase short circuit," *IEEE Trans. Energy Convers.*, vol. 6, no. 1, pp. 62–68, Mar. 1991.
[17] C. Hochgraf and R. H. Lasseter, "Statcom controls for operation with unbalanced voltages," *IEEE Trans. Power Del.*, vol. 13, no. 2, pp. 538–544, Apr. 1998.
[18] B. Charmers and A. C. Williamson, *A. C. Machines Electromagnetics and Design*. Chichester, U.K.: Wiley, 1991, pp. 52–55.

Dawei Xiang was born in Sichuan, China. He received the B.Eng. and M.Sc. degrees in electrical machinery and apparatus from the School of Electrical Engineering, Chongqing University, China, in 1999 and 2000, respectively.

He was an exchange student to the University of Electro-Communications, Tokyo, Japan, from October 1999 to September 2000. In 2004, he was a Visiting Scholar at Durham University, Durham, U.K. Currently, he is a Lecturer of electrical machinery and apparatus at the School of Electrical Engineering, Chongqing University. His research interests include the control of doubly fed electrical machines as used in renewable energy systems.

Li Ran (M'98) received the Ph.D. degree from Chongqing University, Chongqing, China, in 1989, in power systems engineering.

Currently, he is a Lecturer in electrical power and control at the School of Engineering, University of Durham, Durham, U.K. He participated in the commissioning of the Gezhouba-Shanghai HVDC system in China, in 1989. His research interests include application and control of power electronic technologies in power systems and renewable energy systems such as wave and wind energy converters.

Dr. Ran received the Stanley Gray Award—Offshore Technology, from the Institute of Marine Engineers, London, U.K., in 1999, for his study on interconnection of offshore oil rigs.

Peter J. Tavner received the M.A. degree in engineering sciences from Cambridge University, Cambridge, U.K., in 1969, and the Ph.D. degree from Southampton University, Southampton, U.K., in 1978.

Currently, he is a Professor of new and renewable energy at the School of Engineering, University of Durham, Durham, U.K. He has held a number of research and technical positions in the industry including those of the Technical Director of Laurence, Scott & Electromotors Ltd., Norfolk, U.K. and Brush Electrical Machines Ltd., Loughborough, U.K. He was also the Group Technical Director of FKI-DeWind Energy Technology, Loughborough, U.K. His research interests include electrical machines for the extraction of energy from renewable sources and their connection to electricity systems, electromagnetic analysis, the application of condition monitoring to electrical systems, and the use of converters with electrical machines.

Dr. Tavner is a receipient of the Institution Premium Award of the Institution of Electrical Engineers, U.K.

Shunchang Yang was born in Shanghai, China. He received the Graduation degree from the Electrical Engineering Department, Chongqing University, Chongqing, China, in 1960.

In 1960, he was an Assistant Lecturer at the Electrical Engineering Department. From 1985 to 1986, he was a Visiting Scholar at Tennessee University, Knoxville. Since 1988, he has been a Professor at Chongqing University. In 1991, he was at the Kiev Institute of Technology, Kiev, Ukraine and the All Soviet Union Institute of Electrical Engineering and Sciences, Moscow, Russia, in an international project entitled "Asynchronized Synchronous Machines and their Applications in Power Systems." His research interests include design and control of electrical machines of new topologies.